erratum

Benzodiazepine actions mediated by specific γ-aminobutyric acid$_A$ receptor subtypes

Uwe Rudolph, Florence Crestani, Dietmar Benke, Ina Brünig, Jack A. Benson, Jean-Marc Fritschy, James R. Martin, Horst Bluethmann & Hanns Möhler

Nature **401,** 796–800 (1999)

The quality of Fig. 2 was unsatisfactory as published. The figure is reproduced again here. □

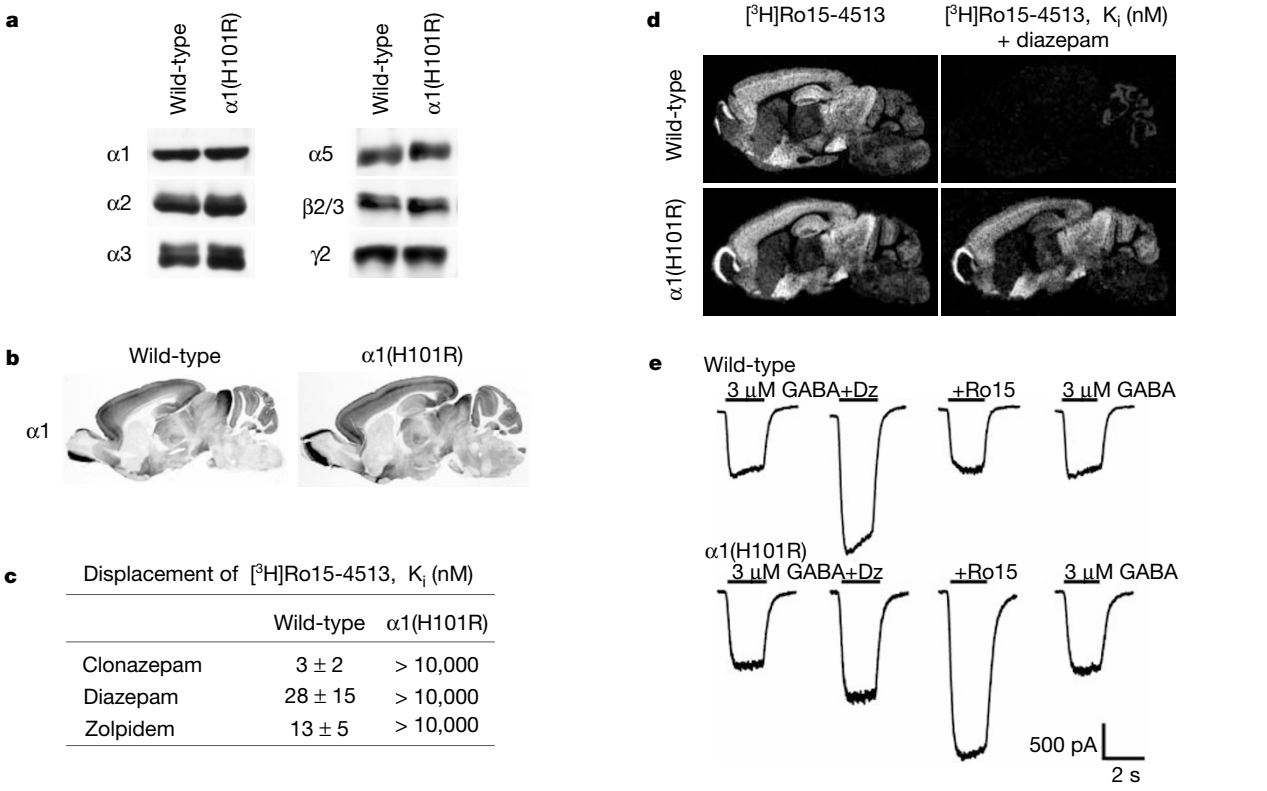

c Displacement of [^{3}H]Ro15-4513, K_i (nM)

	Wild-type	α1(H101R)
Clonazepam	3 ± 2	> 10,000
Diazepam	28 ± 15	> 10,000
Zolpidem	13 ± 5	> 10,000

correction

Observation of a square flux-line lattice in the unconventional superconductor Sr_2RuO_4

T. M. Riseman, P. G. Kealey, E. M. Forgan, A. P. Mackenzie, L. M. Galvin, A. W. Tyler, S. L. Lee, C. Ager, D. McK. Paul, C. M. Aegerter, R. Cubitt, Z. Q. Mao, T. Akima & Y. Maeno

Nature **396,** 242–245 (1998)

In this Letter, the X-ray Laue patterns used to give the orientation of our crystal were misinterpreted by 45°. With the magnetic field perpendicular to the RuO_2 planes, the nearest-neighbour directions in the square flux-line lattice (FLL) are actually at 45° to the Ru–O–Ru directions in the crystal lattice.

Our values of the superconducting parameters λ and ξ still suggest that pairing occurs primarily on the electrons on the γ-sheet of the Fermi surface under the conditions of the experiment. However, the orientation of the FLL, interpreted within Agterberg's two-component Ginzburg–Landau (TCGL) theory[1,2], is no longer consistent with γ-band pairing if we take the values of Fermi surface anisotropy used in refs 1, 2, and obtained by recent band structure calculations[3]. However, other calculations (T. Oguchi, private communication) give a different sign of Fermi surface anisotropy. TCGL theory predictions may be modified by extra anisotropy of the superconducting energy gap[3], by substantial pairing on the α- and/or β-sheets[4] or by anisotropy in the electron mass enhancement. Within TCGL theory, the orientation of the FLL that we observe is no longer consistent with the basal plane anisotropy of H_{c2} at low temperatures in a pure sample[5]. H_{c2} is observed to be larger with the field in a {110} direction than a {100}. The nature of the pairing in Sr_2RuO_4 may be more complicated than we suggested previously.

1. Agterberg, D. F. *Phys. Rev. Lett.* **80,** 5184–5187 (1998).
2. Agterberg, D. F. *Phys. Rev. B* **58,** 14484–14489 (1998).
3. Mazin, I. I., Papaconstantopoulos, D. A. & Singh, D. J. Preprint cond-mat/9907442 at ⟨http://xxx.lanl.gov⟩ (1999).
4. NishiZaki, S., Maeno, Y. & Mao, Z. *J. Low Temp. Phys.* **117,** 1581 (1999).
5. Mao, Z. Q., Maeno, Y., Nishizaki, S., Akima, T. & Ishiguro, T. *Phys. Rev. Lett.* **84,** 991–994 (2000).

The neurons were visualized by phase-contrast microscopy with an inverted microscope (Nikon Diaphot) while recording (in voltage clamp unless otherwise stated ($V_c = -70$ mV) and stimulation (1 ms, +100 mV step depolarization in voltage clamp) was performed using patch-clamp amplifiers (Axopatch 200B, Axon) interfaced with a PC. Signals filtered at 5 kHz using amplifier circuitry were sampled at 10 kHz and analysed using Axoscope software (Axon). Series resistance (10–30 MΩ) was always compensated at 80% (lag 100 μs). For assaying synaptic connectivity, each neuron was stimulated at a low frequency (0.03–0.06 Hz), and the responses from the other neurons as well as autaptic responses in the stimulated neuron itself were recorded (see Fig. 4). Monosynaptic currents had onset latencies <4 ms (ref. 29). Polysynaptic currents had onset latencies ≥6 ms and often exhibited multiple components, with frequent failure for some PSC components to occur during the test stimulation. *P* of an identified component is measured based on its response to 50–100 consecutive test stimuli (0.05 Hz unless otherwise indicated). For polysynaptic pathways in these cultures, each additional synapse usually introduced a delay of 4–10 ms (2–5 ms for synaptic delay and action-potential conduction and 2–5 ms delay for the initiation of an action potential). Neurons in these cultures were either glutamate-mediating or GABA-mediating in nature and could be identified based on the time course, reversal potential and pharmacology of their evoked synaptic currents (EPSCs and IPSCs, respectively)[13,29]. EPSCs were blocked by 10 μM 6-cyano-7-nitroquinoxaline-2,3-dione (CNQX, RBI) whereas IPSCs were blocked by 10 μM bicuculline (RBI). The IPSCs had distinctly longer decay time and more negative reversal potentials (around −50 mV) than EPSCs. In a typical culture, we estimated that less than 20% of the neurons were GABA-mediated.

Received 29 June; accepted 20 August 1999.

1. Katz, L. C. & Shatz, C. J. Synaptic activity and the construction of cortical circuits. *Science* **274,** 1133–1138 (1996).
2. Abbott, L. F., Varela, J. A., Sen, K. & Nelson, S. B. Synaptic depression and cortical gain control. *Science* **275,** 220–224 (1997).
3. Squire, L. R. *Memory and Brain* (Oxford Univ. Press, New York, 1987).
4. Churchland, P. S. & Sejnowski, T J. *the Computational Brain* (The MIT Press, Cambridge, MA, 1992).
5. Bliss, T. V. & Collingridge, G. L. A synaptic model of memory: long-term potentiation in the hippocampus. *Nature* **361,** 31–39 (1993).
6. Goda, Y. & Stevens, C. F. Synaptic plasticity: the basis of particular types of learning. *Curr. Biol.* **6,** 375–378 (1996).
7. Levy, W. B. & Steward, O. Temporal contiguity requirements for long-term associative potentiation/depression in the hippocampus. *Neuroscience* **8,** 791–797 (1983).
8. Markram, H., Lubke, J., Frotscher, M. & Sakmann, B. Regulation of synaptic efficacy by coincidence of postsynaptic APs and EPSPs. *Science* **275,** 213–215 (1997).
9. Magee, J. C. & Johnston, D. A synaptically controlled, associative signal for Hebbian plasticity in hippocampal neurons. *Science* **275,** 209–213 (1997).
10. Bell, C. C., Han, V. Z., Sugawara, Y. & Grant, K. Synaptic plasticity in a cerebellum-like structure depends on temporal order. *Nature* **387,** 278–281 (1997).
11. Debanne, D., Gahwiler, B. H. & Thompson, S. M. Long-term synaptic plasticity between pairs of individual CA3 pyramidal cells in rat hippocampal slice cultures. *J. Physiol. (Lond.)* **507,** 237–247 (1998).
12. Zhang, L. I., Tao, H. W., Holt, C. E., Harris, W. A. & Poo, M.-m. A critical window for cooperation and competition among developing retinotectal synapses. *Nature* **395,** 37–44 (1998).
13. Bi, G.-q. & Poo, M.-m. Synaptic modifications in cultured hippocampal neurons: dependence on spike timing, synaptic strength, and postsynaptic cell type. *J. Neurosci.* **18,** 10464–10472 (1998).
14. Hopfield, J. J. Pattern recognition computation using action potential timing for stimulus representation. *Nature* **376,** 33–36 (1995).
15. Singer, W. & Gray, C. M. Visual feature integration and the temporal correlation hypothesis. *Annu. Rev. Neurosci.* **18,** 555–86 (1995).
16. Gerstner, W., Kempter, R., van Hemmen, J. L. & Wagner, H. A neuronal learning rule for sub-millisecond temporal coding. *Nature* **383,** 76–81 (1996).
17. Strong, S. P., Koberle, R., De Ruyter Van Steveninck, R. R. & Bialek, W. Entropy and information in neural spike trains. *Phys. Rev. Lett.* **80,** 197–200 (1998).
18. Malenka, R. C. & Nicoll, R. A. NMDA-receptor-dependent synaptic plasticity: multiple forms and mechanisms. *Trends Neurosci.* **16,** 521–527 (1993).
19. Linden, D. J. & Connor, J. A. Long-term synaptic depression. *Annu. Rev. Neurosci.* **18,** 319–357 (1995).
20. Miles, R. & Wong, R. K. Latent synaptic pathways revealed after tetanic stimulation in the hippocampus. *Nature* **329,** 724–726 (1987).
21. Turrigiano, G., Abbott, L. F. & Marder, E. Activity-dependent changes in the intrinsic properties of cultured neurons. *Science* **264,** 974–977 (1994).
22. Buzsàki, G. Polysynaptic long-term potentiation: a physiological role of the perforant path–CA3/CA1 pyramidal cell synapse. *Brain Res.* **455,** 192–195 (1988).
23. Buonomano, D. V., Hickmott, P. W. & Merzenich, M. M. Context-sensitive synaptic plasticity and temporal-to-spatial transformations in hippocampal slices. *Proc. Natl Acad. Sci. USA* **94,** 10403–10408 (1997).
24. Carr, C. E. & Konishi, M. A circuit for detection of interaural time differences in the brain stem of the barn owl. *J. Neurosci.* **10,** 3227–3246 (1990).
25. Kristan, W. B J. He's got rhythm: single neurons signal timing on a scale of seconds. *Nature Neurosci.* **1,** 643–645 (1998).
26. Tank, D. W. & Hopfield, J. J. Neural computation by concentrating information in time. *Proc. Natl Acad. Sci. USA* **84,** 1896–1900 (1987).
27. Moore, J. W., Choi, J.-S. & Brunzell, D. H. in *Timing of Behaviour* (eds Risenbaum, D. A. & Collyer, C. E.) 3–34 (MIT Press, Cambridge, MA, 1998).
28. Abeles, M. *Corticonics* (Cambridge Univ. Press, Cambridge, 1991).
29. Fitzsimonds, R. M., Song, H. J. & Poo, M.-m. Propagation of activity-dependent synaptic depression in simple neural networks. *Nature* **388,** 439–448 (1997).
30. Rae, J., Cooper, K., Gates, P. & Watsky, M. Low access resistance perforated patch recordings using amphotericin B. *J. Neurosci. Methods* **37,** 15–26 (1991).

Supplementary information is available on *Nature*'s World-Wide Web site (http://www.nature.com) or as paper copy from the London editorial office of *Nature*.

Acknowledgements

We thank X. Wang for culture preparations and B. Berninger, W. Kristan, L. Zhang, A. Schinder and S. Andersen for helpful discussions and comments on the manuscript. Supported by grants from NIH (M.P.) and a President's Postdoctoral Fellowship from the University of California and a training grant from NIH (G.B.).

Correspondence and requests for materials should be addressed to G.B. (e-mail: gbi@ucsd.edu).

Benzodiazepine actions mediated by specific γ-aminobutyric acid$_A$ receptor subtypes

Uwe Rudolph*, Florence Crestani*, Dietmar Benke*, Ina Brünig*, Jack A. Benson*, Jean-Marc Fritschy*, James R. Martin†, Horst Bluethmann† & Hanns Möhler*

** Institute of Pharmacology, University of Zürich, and Swiss Institute of Technology (ETH), Winterthurestrasse 190, CH-8057 Zürich, Switzerland*
† Pharma Division, Preclinical Research, F. Hoffmann-LaRoche Ltd, CH-4002 Basel, Switzerland

GABA$_A$ (γ-aminobutyric acid$_A$) receptors are molecular substrates for the regulation of vigilance, anxiety, muscle tension, epileptogenic activity and memory functions, which is evident from the spectrum of actions elicited by clinically effective drugs acting at their modulatory benzodiazepine-binding site. Here we show, by introducing a histidine-to-arginine point mutation at position 101 of the murine α1-subunit gene, that α1-type GABA$_A$ receptors, which are mainly expressed in cortical areas and thalamus[1], are rendered insensitive to allosteric modulation by benzodiazepine-site ligands, whilst regulation by the physiological neurotransmitter γ-aminobutyric acid is preserved. α1(H101R) mice failed to show the sedative, amnesic and partly the anticonvulsant action of diazepam. In contrast, the anxiolytic-like, myorelaxant, motor-impairing and ethanol-potentiating effects were fully retained, and are attributed to the nonmutated GABA$_A$ receptors found in the limbic system (α2, α5), in monoaminergic neurons (α3) and in motoneurons (α2, α5)[1]. Thus, benzodiazepine-induced behavioural responses are mediated by specific GABA$_A$ receptor subtypes in distinct neuronal circuits, which is of interest for drug design.

Fast synaptic inhibition in the mammalian brain is largely mediated by the activation of GABA$_A$ receptors, which are heteromeric GABA-gated chloride channels[2]. Their opening frequency is enhanced by agonists of the benzodiazepine site, which is the basis of their therapeutic effectiveness but also of their undesired side effects. The classical benzodiazepines such as diazepam interact indiscriminately with all benzodiazepine-sensitive GABA$_A$ receptor subtypes (α1, α2, α3 and α5) with comparable affinities[3,4]. These receptors have a histidine at a conserved position (α1-H101, α2-H101, α3-H126 and α5-H105). In contrast, the benzodiazepine-insensitive receptor subtypes in the brain (α4 and α6) have an arginine in the corresponding position.

Recombinant diazepam-sensitive receptors can be rendered diazepam-insensitive by replacing this histidine by arginine without altering the GABA sensitivity, as shown for the α1 subunit[5,6] and the α2, α3 and α5 subunits[7]. The pharmacological significance of the predominant GABA$_A$ receptor subtype in the brain, which contains

the α1 subunit[1,8], was evaluated by introducing the α1(H101R) point mutation into the germline of mice by gene targeting ('knock-in'). A replacement vector RV-10, which contained the desired point mutation in exon 4 and a *loxP*-flanked neomycin resistance marker in intron 4, was electroporated into E14 embryonic stem (ES) cells. Correctly targeted ES cells containing the point mutation and the neo marker (Mutant allele 1, Fig. 1a) were injected into blastocysts. Mice carrying this mutant allele were bred to Ella-cre mice[9]. The Ella-cre transgene efficiently eliminated the *loxP*-flanked neomycin resistance cassette from the germ line[9], thus generating Mutant allele 2 (Fig. 1a), which was bred on different backgrounds and used in all subsequent experiments. The Ella-cre transgene was bred out. The mutant alleles were confirmed by Southern blotting (Fig. 1b) and sequence analysis (Fig. 1c).

α1(H101R) mice showed no overt distinctive phenotype and bred normally. Immunoblotting confirmed that the mutant α1 subunit and the other major $GABA_A$ receptor subunits (α2, α3, α5, β2/3 and γ2) were expressed in the α1(H101R) mice at normal levels (Fig. 2a). The immunohistochemical distribution of these subunits in α1(H101R) mice was indistinguishable from that of the wild type (see also Fig. 2b). To verify the diazepam-insensitivity of $GABA_A$ α1(H101R) receptors in the central nervous system, $GABA_A$ receptors were immunoprecipitated from detergent extracts of whole brain membranes with an α1-subunit-specific antiserum. The receptors from α1(H101R) mice displayed a ligand-binding profile consistent with that of physiologically diazepam-insensitive $GABA_A$ receptors[10], that is, a virtual lack of affinity for diazepam, clonazepam and zolpidem (Fig. 2c). The diazepam-insensitive sites in α1(H101R) mutant brain were visualized autoradiographically by [^{3}H]Ro15-4513 binding in the presence of 100 μM diazepam in all regions known to express the α1-subunit, including olfactory bulb, cerebral cortex, thalamus, pallidum, midbrain and cerebellum (Fig. 2d). In line with the known abundance of $GABA_A$ α1 receptors, the number of diazepam-insensitive binding sites (B_{max}; [^{3}H]Ro15-4513 binding) increased from 7% in wild-type mice to 66% in α1(H101R) mice without any change in the dissociation constant (K_d). The gating properties of the point-mutated receptor were assessed in whole-cell patch-clamp recordings from acutely dissociated cerebellar Purkinje cells, in which α1 receptors predominate. Although the response to GABA (3 μM) was indistinguishable in cells from α1(H101R) and wild-type mice, potentiation by diazepam (1 μM) was greatly reduced in cells from α1(H101R) mice (Fig. 2e). The remaining potentiation is attributed to diazepam-sensitive receptors other than α1 in these cells. The response to the inverse agonist Ro15-4513 (1 μM) in wild-type cells was switched to an agonistic response in the mutant cells (Fig. 2e), which is in line with its agonistic effect at recombinant α1(H101R) receptors[7].

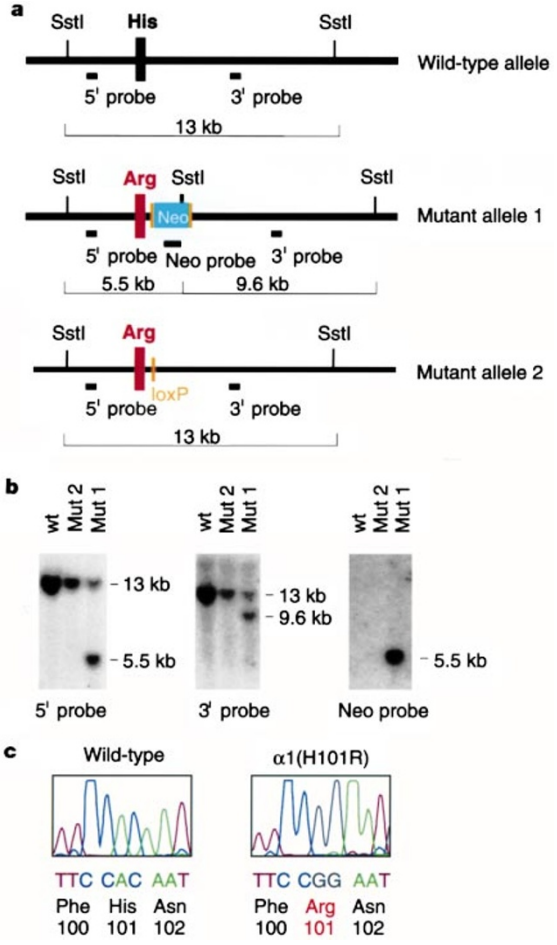

Figure 1 Targeting the $GABA_A$ receptor α1 subunit (GABRA1) gene. **a**, The 5′ and 3′ flanking probes, which contain the genomic sequences directly adjacent to the targeting vector, are depicted as solid bars. His and Arg denote the codons for His 101 and Arg 101 in exon 4 of the wild-type and mutant alleles, respectively. **b**, Southern blot analysis of wild-type (wt) and mutant (Mut) alleles in mice. The genomic DNA was cut with *Sst*I. **c**, Verification of the α1(H101R) point mutation by DNA sequencing. Exon 4 sequences were amplified from mouse genomic DNA by polymerase chain reaction and sequenced using an ABI Prism 310 Genetic Analyzer.

Diazepam and other classical benzodiazepines are widely used clinically as anxiolytics, hypnotics, anticonvulsants and myorelaxants, with side effects including anterograde amnesia, impairment of motor coordination and potentiation of ethanol effects. To identify the role of $GABA_A$ α1 receptors in the actions of diazepam, various drug-induced behavioural responses were compared in α1(H101R) mice and wild-type mice. Diazepam depressed motor activity, a measure of sedation, in wild-type but not in α1(H101R) mice ($F(3, 120) = 4.90$, $P < 0.01$) (Fig. 3a). α1(H101R) mice were also resistant to the sedative effect of zolpidem[11] (60 mg kg^{-1} orally (p.o.)), a ligand with preferential affinity for $GABA_A$ α1 receptors. The sedative or hypnotic effects of drugs other than ligands of the benzodiazepine site were unaltered in α1(H101R) mice. The neurosteroid 3α-hydroxy-5β-pregnan-20-one (100 mg kg^{-1} p.o.)[12] decreased motor activity to the same extent in α1(H101R) and wild-type mice. Similarly, sodium pentobarbital, at the minimally effective dose of 100 mg kg^{-1} intraperitoneally (i.p.), induced loss of righting reflex with the same latency in both genotypes. These results indicate that the lack of drug-induced sedation in α1(H101R) mice is restricted to benzodiazepine-site ligands.

The memory impairing effect of diazepam was analysed in the step-through passive avoidance paradigm following administration of the drug 30 min before the training session[13]. The latency for re-entering the dark compartment 24 h later was shortened in wild-type ($U = 16.5$, $P < 0.01$ compared with vehicle) but not in α1(H101R) mice ($U = 48.0$, n.s.) (Fig. 3b). In a modified lick suppression paradigm[14], the latency to drink the first 100 licks was measured before a training session of punished drinking under vehicle or diazepam treatment (10 mg kg^{-1} i.p.) and reassessed three days later (recall session) under drug-free conditions. Wild-type mice trained under vehicle displayed an enhanced recall latency (median (range): 928s (64–1,200) compared with a training latency of 12s (10–99), $P < 0.05$, $n = 7$). In contrast, wild-type mice trained under diazepam showed a short recall latency (13s (12–1,200) compared with a training latency of 29s (12–200), $n = 6$)), suggesting a drug-induced amnesia. In both vehicle- and diazepam-treated α1(H101R) mice, the recall latency (vehicle 1,200s (12–1,200), $n = 7$; diazepam 1,200s (45–1,200), $n = 6$) was enhanced compared with the training latency (vehicle 34s (14–62); diazepam 11s (10–28), $P < 0.05$). All four groups of mice afflicted on

themselves a similar amount of punished licks during the training session, making a potential analgesic effect of diazepam unlikely. Thus, two different paradigms point to the absence of the amnesic effect of diazepam in α1(H101R) mice. In contrast, the muscarinic antagonist, scopolamine (1.5 mg kg^{-1} i.p.), had an amnesic effect in both α1(H101R) mice (latency 42.7 ± 22.7 s compared with vehicle: 165.8 ± 14.2 s, $n = 5$–8, $P < 0.01$) and wild-type mice (latency 50.2 ± 26.8 s compared with vehicle: 180.0 ± 0 s, $n = 4$–8, $P < 0.05$) in the passive avoidance protocol. These results underline the specificity of the $GABA_A$ α1 receptor in mediating diazepam-induced amnesia.

The anticonvulsant activity of diazepam was assessed against pentylenetetrazole-induced tonic convulsions[15]. It was reduced in α1(H101R) mice ($\chi^2(4) = 12.50$, $P < 0.05$) compared with wild-type mice ($\chi^2(4) = 27,76$, $P < 0.001$). Indeed, 30 mg kg^{-1} diazepam protected all wild-type mice whereas 45.5% of α1(H101R) mice still developed tonic seizures (Fig. 3c). The anticonvulsant effect of diazepam which remained in α1(H101R) mice was due to $GABA_A$

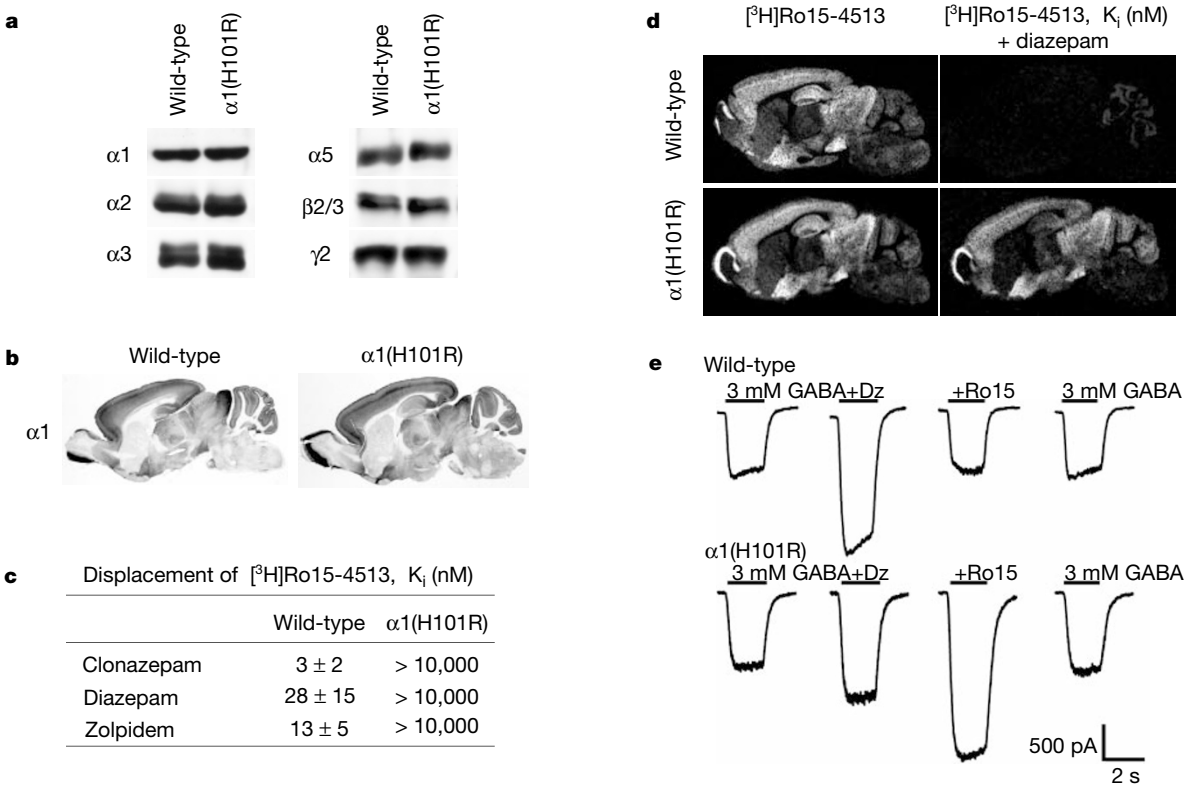

Figure 2 Biochemical, morphological and electrophysiological characteristics of $GABA_A$ receptors in α1(H101R) mice. **a**, Western blots of $GABA_A$ receptor subunit proteins in wild-type and α1(H101R) mice with antisera recognizing $GABA_A$ receptor subunits α1, α2, α3, α5, β2/3 and γ2. **b**, Immunohistochemical regional distribution of the α1 subunit in parasagittal brain sections from wild-type (left) and α1(H101R) mice (right). **c**, Displacement potencies of several benzodiazepine-site ligands at wild-type and α1(H101R) receptors, immunoprecipitated with an α1-subunit-specific antiserum. **d**, Autoradiographic distribution of total [^{3}H]Ro15-4513-binding sites (left) and diazepam-insensitive [^{3}H]Ro15-4513-binding sites (right) in wild-type mice (top) and α1(H101R) mice (bottom). Parasagittal brain sections were incubated with 20 nM [^{3}H]Ro15-4513 in the absence (left) or presence of 100 μM diazepam (right). Low levels of diazepam-insensitive binding in wild-type mice represent the receptors containing the α4 or α6 subunit. **e**, Patch-clamp analysis of GABA responses in dissociated cerebellar Purkinje cells. The potentiation by diazepam (Dz) was 134 ± 19% (mean ± s.e.m.; $n = 12$) in cells of wild-type mice and was reduced to 71 ± 14% ($n = 10$) in cells of α1(H101R) mice ($P < 0.05$, t-test). The inverse agonist Ro15-4513 (Ro15) displayed an agonistic response in the mutant cells.

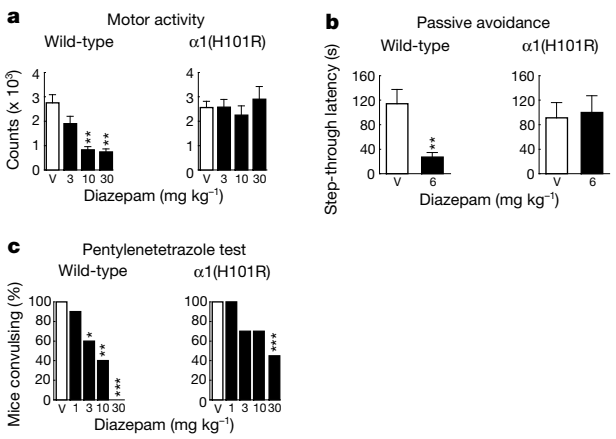

Figure 3 Behavioural assessment of drug-induced sedation, amnesia and anticonvulsant activity in wild-type and α1(H101R) mice. **a**, Diazepam induced a dose-dependent decrease in motor activity in wild-type but not in α1(H101R) mice ($n = 16$ per group). **b**, In a passive avoidance paradigm, diazepam shortened the latency to re-enter the dark compartment 24 h after training in wild-type mice but not in α1(H101R) mice ($n = 10$ per group). **c**, Partial anticonvulsant activity of diazepam against pentylenetetrazole (120 mg kg^{-1} i.p.) in α1(H101R) compared with wild-type mice ($n = 10$–11 per group). All results are given as means ± s.e.m. Asterisk, $P < 0.05$; double asterisks, $P < 0.01$; triple asterisks, $P < 0.001$. Diazepam was administered p.o.; V, vehicle.

receptors other than α1, as it was antagonized by the benzodiazepine antagonist, flumazenil[16]. Furthermore, sodium phenobarbital was fully effective as an anticonvulsant in α1(H101R) mice with a dose–response relationship similar to that of wild-type mice. These results show that the anticonvulsant activity of benzodiazepine site ligands is partly mediated by $GABA_A$ α1 receptors.

In striking contrast, the myorelaxant, motor-impairing, ethanol-potentiating and anxiolytic-like properties of diazepam were not impaired in the α1(H101R) mice, indicating that they may be exclusively mediated by $GABA_A$ receptors of the α2, α3 and/or α5 type. Diazepam reduced muscle tone to the same extent in wild-type ($\chi^2(4) = 32.24$, $P < 0.001$) and α1(H101R) mice ($\chi^2(4) = 33.17$, $P < 0.001$) as indicated by a dose-dependent increase in the number of mice with impaired grasping reflex in the horizontal wire test[15] (Fig. 4a). This myorelaxant effect was antagonized by flumazenil. In the rotarod test[15], both α1(H101R) and wild-type mice displayed a dose-dependent motor impairment (Treatment, $F(2, 54) = 14.82$, $P < 0.001$, analysis of variance (ANOVA) with repeated measures on the same subjects) (Fig. 4b). Furthermore, diazepam potentiated in a dose-dependent manner the sedative effect of ethanol by increasing the duration of the loss of the righting reflex[17] in both wild-type and α1(H101R) mice (Treatment, $F(3, 76) = 12.10$, $P < 0.001$) (Fig. 4c). Finally, the anxiolytic-like activity of diazepam appeared unaltered, as assessed in two classical paradigms. In the light/dark choice test[18], diazepam dose-dependently increased the time spent in the illuminated area in wild-type and α1(H101R) mice (Treatment, $F(2, 54) = 10.55$, $P < 0.001$) (Fig. 4d) without affecting the number of transitions. Likewise, in the elevated X-maze[19], diazepam significantly increased the number of open arm entries for both wild-type and α1(H101R) mice ($F(3, 68) = 3.93$, $P < 0.05$) (Fig. 4e). The increase in open arm entries seen in α1(H101R) mice up to 2 mg kg^{-1} was maintained only up to 1 mg kg^{-1} in wild-type mice, presumably because of the susceptibility to sedation (Fig. 3a) of wild-type but not α1(H101R) mice.

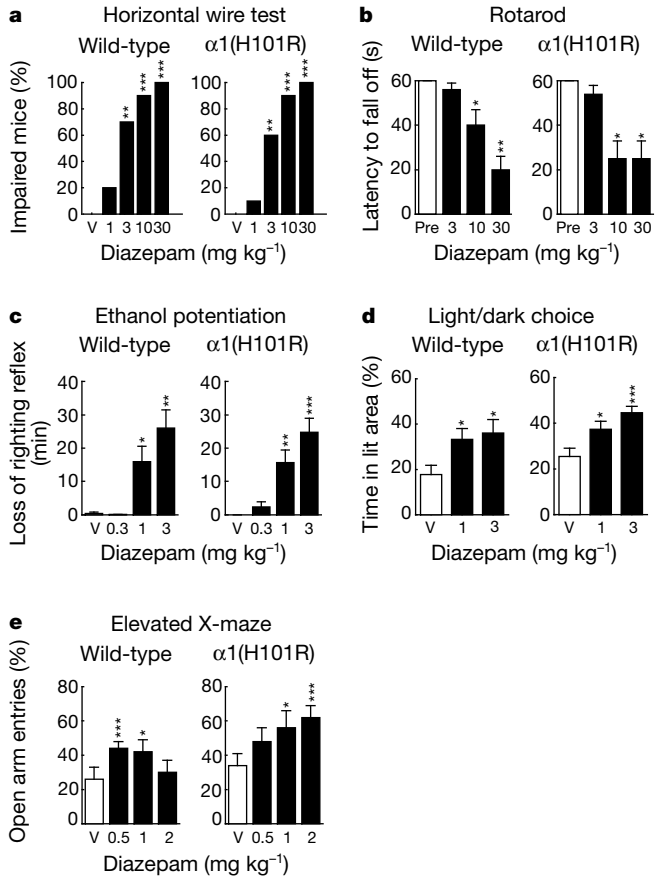

Figure 4 Behavioural assessment of myorelaxant, motor-impairing, ethanol-potentiating and anxiolytic-like actions of diazepam in wild-type and α1(H101R) mice. **a**, Dose-dependent impairment of the grasping reflex in wild-type and α1(H101R) mice ($n = 10$–11 per group). **b**, Dose-dependent decrease of the latency to fall off the rotating rod in wild-type and α1(H101R) mice ($n = 10$ per group). **c**, Dose-dependent potentiation of the sedative effect of a 15% ethanol solution in wild-type and α1(H101R) mice ($n = 5$–15 per group). **d**, Dose-dependent increase of the percentage of time spent in the lit area in wild-type and α1(H101R) mice ($n = 10$ per group) tested in a light/dark choice paradigm. **e**, Dose-dependent increase of the number of open arm entries (in percentage of total number of arm entries) in both wild-type and α1(H101R) mice ($n = 8$–11 per group) exposed to an elevated X-maze. Results are given as means ± s.e.m. Asterisks, $P < 0.05$; double asterisks, $P < 0.01$; triple asterisks, $P < 0.001$. Diazepam was administered p.o.; V, vehicle.

Table 1 Roles of $GABA_A$ receptor subtypes in benzodiazepine action

	α1	α2, α3, α5
Sedation	+	–
Amnesia	+	–
Seizure protection	+	+
Anxiolysis	–	+
Myorelaxation	–	+
Motor impairment	–	+
Ethanol potentiation	–	+

Our finding that benzodiazepine actions are mediated by specific $GABA_A$ receptor subtypes points to new strategies for drug design for several therapeutic indications. For example, agonists acting on α2, α3, and/or α5 but not on α1 receptors are expected to be nonsedative and nonamnesic anxiolytics (Table 1). Furthermore, the α1(H101R) mice provide a suitable model to investigate whether the development of tolerance and dependence liability of benzodiazepines is also subtype specific. In addition, our results are likely to be of physiological relevance, as benzodiazepine agonists act by enhancing physiological GABA-mediated transmission. It is therefore conceivable that the physiological regulation of vigilance and memory function is mediated by circuits involving GABA-mediated transmission at α1 receptors, whereas neurons with benzodiazepine-sensitive $GABA_A$ receptors other than α1 are involved in regulating anxiety. Thus, $GABA_A$ receptor subtypes promise to define circuits mediating distinct behaviours. □

Methods

Strain background of mice

α1(H101R) chimaeras were crossed first to Ella-cre mice (third backcross to 129/SvEv), to remove the neo cassette from the germline[9] through *cre/loxP*-mediated excision, twice more to 129/SvEv mice and then for five generations to both 129/SvJ and C57BL/6J. Heterozygote crosses were set up for each strain to yield homozygous mutant, heterozygous and wild-type mice. Typically, 20–25 breeding pairs of both homozygous mutant and wild-type mice produced the experimental animals which were used at roughly 8–12 weeks of age. Each mouse was injected with diazepam only once.

Behavioural tests

All tests were performed in two backgrounds: motor activity, pentylenetetrazole test, horizontal wire test, rotarod and ethanol potentiation in 129/SvEv (Fig. 3a, c, d) and 129/SvJ (Fig. 4b); passive avoidance and elevated X-maze in 129/SvJ (Fig. 3b) and C57BL/6J (Fig. 4e); light/dark choice test in 129/SvJ (Fig. 4d) and in 129/SvJ × C57BL/6J F1 hybrids. The 129/SvEv background was used for binding studies, autoradiography, immunoprecipitation and immunohistochemistry, the 129/SvJ background for electrophysiology.

Received 2 June; accepted 31 August 1999.

1. Fritschy, J. M. & Mohler, H. $GABA_A$-receptor heterogeneity in the adult rat brain: differential regional and cellular distribution of seven major subunits. *J. Comp. Neurol.* **359,** 154–194 (1995).
2. Barnard, E. A. *et al.* International Union of Pharmacology. XV. Subtypes of γ-aminobutyric $acid_A$ receptors: classification on the basis of subunit structure and receptor function. *Pharmacol. Rev.* **50,** 291–313 (1998).

3. Mohler, H. & Okada, T. Benzodiazepine receptor: demonstration in the central nervous system. *Science* **198,** 849–851 (1977).
4. Braestrup, C., Albrechtsen, R. & Squires, R. F. High densities of benzodiazepine receptors in human cortical areas. *Nature* **269,** 702–704 (1977).
5. Wieland, H. A., Lüddens, H. & Seeburg, P. H. A single histidine in $GABA_A$ receptors is essential for benzodiazepine agonist binding. *J. Biol. Chem.* **267,** 1426–1429 (1992).
6. Kleingoor, C., Wieland, H. A., Korpi, E. R., Seeburg, P. H. & Kettenmann, H. Current potentiation by diazepam but not GABA sensitivity is determined by a single histidine residue. *Neuroreport* **4,** 187–190 (1993).
7. Benson, J. A., Löw, K., Keist, R., Mohler, H. & Rudolph, U. Pharmacology of recombinant γ-aminobutyric $acid_A$ receptors rendered diazepam-insensitive by point-mutated α-subunits. *FEBS Lett.* **431,** 400–404 (1998).
8. Fritschy, J.-M. *et al.* Five subtypes of type A γ-aminobutyric acid receptors identified in neurons by double and triple immunofluorescence staining with subunit-specific antibodies. *Proc. Natl Acad. Sci. USA* **89,** 6726–6730 (1992).
9. Lakso, M. *et al.* Efficient *in vivo* manipulation of mouse genomic sequences at the zygote stage. *Proc. Natl Acad. Sci. USA* **93,** 5860–5865 (1996).
10. Knoflach, F. *et al.* Pharmacological modulation of the diazepam-insensitive recombinant γ-amino-butyric $acid_A$ receptors α4β2γ2 and α6β2γ2. *Mol. Pharmacol.* **50,** 1253–1261 (1996).
11. Bernard, F. *et al.* in *Zolpidem: an Update of its Pharmacological Properties and the Therapeutic Place in the Management of Insomnia* (eds Freeman, H., Puech, A. J. & Roth, T.) 21–31 (Elsevier, Paris, 1996).
12. Melchior, C. L. & Allen, P. M. Interaction of pregnanolone and pregnanolone sulfate with ethanol and pentobarbital. *Pharmacol. Biochem. Behav.* **42,** 605–611 (1992).
13. Beuzen, A. & Belzung, C. Link between emotional memory and anxiety states: a study by principal component analysis. *Physiol. Behav.* **58,** 111–118 (1995).
14. Vogel, J. R., Beer, B. & Clody, D. E. A simple and reliable conflict procedure for testing anti-anxiety agents. *Psychopharmacology* **21,** 1–7 (1971).
15. Bonetti, E. P. *et al.* Benzodiazepine antagonist Ro 15-1788: neurological and behavioral effects. *Psychopharmacology* **78,** 8–18 (1982).
16. Hunkeler, W. *et al.* Selective antagonists of benzodiazepines. *Nature* **290,** 514–516 (1981).
17. Bonetti, E. P. *et al.* Ro 15-4513: Partial inverse agonism at the BZR and interaction with ethanol. *Pharmacol. Biochem. Behav.* **31,** 733–749 (1988).
18. Misslin, R., Belzung, C. & Vogel, E. Behavioural validation of a light/dark choice procedure for testing anti-anxiety agents. *Behav. Proc.* **18,** 119–132 (1989).
19. Lister, R. G. The use of a plus-maze to measure anxiety in the mouse. *Psychopharmacology* **92,** 180–185 (1987).

Supplementary information is available on *Nature*'s World-Wide Web site (http://www.nature.com) or as paper copy from the London editorial office of *Nature*.

Acknowledgements

We thank Y. Lang for blastocyst injections, D. Blaser, S. Ganz, H. Pochetti and G. Schmid for animal care, R. Keist and C. Michel for technical assistance and H. Westphal for providing Ella-cre mice. This work was supported by a grant from the Swiss National Science Foundation.

Correspondence and requests for materials should be addressed to U.R. (e-mail: rudolph@pharma.unizh.ch).

P/Q-type calcium channels mediate the activity-dependent feedback of syntaxin-1A

Kathy G. Sutton*†, John E. McRory*†, Heather Guthrie*, Timothy H. Murphy‡ & Terrance P. Snutch*

** Biotechnology Laboratory and ‡ Kinsmen Laboratory of Neurological Research, Dept Psychiatry University of British Columbia, Vancouver, V6T 1Z3, Canada*
† These authors contributed equally to this work.

Spatial and temporal changes in intracellular calcium concentrations are critical for controlling gene expression in neurons[1–5]. In many neurons, activity-dependent calcium influx through L-type channels stimulates transcription that depends on the transcription factor CREB by activating a calmodulin-dependent pathway[6–11]. Here we show that selective influx of calcium through P/Q-type channels[12–14] is responsible for activating expression of syntaxin-1A, a presynaptic protein that mediates vesicle docking, fusion and neurotransmitter release. The initial P/Q-type calcium signal is amplified by release of calcium from intracellular stores and acts through phosphorylation that is dependent on the calmodulin-dependent kinase CaM K II/IV, protein kinase A and mitogen-activated protein kinase kinase. Initiation of syntaxin-1A expression is rapid and short-lived, with syntaxin-1A ultimately interacting with the P/Q-type calcium channel to decrease channel availability. Our results define an activity-dependent feedback pathway that may regulate synaptic efficacy and function in the nervous system.

Syntaxin-1A interacts with the synaptic core (SNARE) complex and is tightly regulated by a number of proteins including munc-13, munc-18 and tomosyn[15–18]. Syntaxin-1A also binds to the domain II–III linker of N- and P/Q-type voltage-gated Ca^{2+} channels and shifts current inactivation properties to more negative potentials[19–23]. Transient expression of human α_{1A} (P/Q-type) Ca^{2+} channels in HEK293 cells resulted in a relatively negative steady-state inactivation (SSI) and indicated that there may be a corresponding interaction with syntaxin (Fig. 1a; voltage for 50% inactivation ($V50_{inact}$) $= -69.2 \pm 1.6$ mV, $n = 17$). Incubation with botulinum toxin C1 (200–400 ng ml^{-1} for 24 h) to cleave syntaxin[24] made the SSI ~10 mV more depolarized (Fig. 1a; $V50_{inact} = 59.7 \pm 1.7$ mV, $P < 0.001$, $n = 11$). Treatment with botulinum C1 toxin did not affect the voltage-dependence of current activation (Fig. 1a inset). To confirm the presence of syntaxin, cells were co-transfected with an antisense syntaxin construct directed against the first 338 bases of rat syntaxin (GenBank accession code M95734; 90% identical with human syntaxin-1A), which resulted in a depolarizing shift in the SSI curve (Fig. 1b; $V50_{inact} = -63.1 \pm 1.3$ mV, $P < 0.01$, $n = 18$). Thus, syntaxin-1A endogenous to HEK293 cells interacts with transiently expressed α_{1A} P/Q-type Ca^{2+} channels and shifts the channels into a more inactivated state.

Unexpectedly, western blot analysis using a monoclonal antibody against human syntaxin-1A[25] showed that syntaxin-1A was not endogenously expressed in HEK293 cells (Fig. 2a); however, a 34–36 kilodalton band that co-migrated with syntaxin-1A protein was detected in HEK293 cells transfected with the α_{1A} P/Q-type Ca

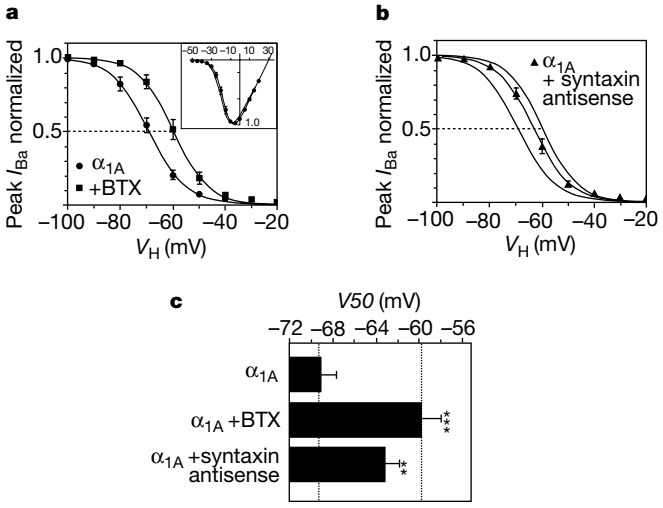

Figure 1 Interaction of syntaxin with α_{1A} P/Q-type channels induces a negative shift in steady-state inactivation (SSI). **a**, Cells were held at the holding voltage (V_H) for 15 s before activation; command voltage (V_c) = 0 mV. Data were normalized to the maximum current ($V_H = -120$ mV) and fitted using $y = 1/(1 + \exp((V50_{inact} - x)/k))$. Botulinum toxin (BTX) shifts $V50_{inact}$ to a more depolarized value without any change in the slope ($k = -5.6 \pm 0.2$, $P = 0.42$). **b**, Antisense syntaxin-1A induces a depolarizing shift in the SSI of α_{1A}. Dashed lines represent fits in (**a**). **c**, Summary of mean (±s.e.m.) $V50_{inact}$. ** = $P < 0.01$ and *** = $P < 0.001$ compared with α_{1A} control. I_{Ba}, maximum peak current.

3. Warren, W. S., Rabitz, H. & Dahleh, M. Coherent control of quantum dynamics: the dream is alive. *Science* **259,** 1581–1589 (1993).
4. Weiner, A. M. & Heritage, J. P. Picosecond and femtosecond Fourier pulse shape synthesis. *Rev. Phys. Appl.* **22,** 1619–1628 (1987).
5. Weiner, A. M., Leaird, D. E., Patel, J. S & Wullert, J. R. Programmable femtosecond pulse shaping by use of a multielement liquid-crystal phase modulator. *Opt. Lett.* **15,** 326–328 (1990).
6. Hillegas, C. W., Tull, J. X., Goswami, D., Strickland, D. & Warren, W. S. Femtosecond laser pulse shaping by use of microsecond radio-frequency pulses. *Opt. Lett.* **19,** 737–739 (1994).
7. Wefers, M. M. & Nelson, K. A. Generation of high-fidelity programmable ultrafast optical waveforms. *Opt. Lett.* **20,** 1047–1049 (1995).
8. Tannor, D. J. in *Molecules in Laser Fields* (ed. Bandrauk, A.) 403–446 (Dekker, New York, 1994).
9. Tannor, D. J. & Rice, S. A. Control of selectivity of chemical reaction via control of wave packet evolution. *J. Chem. Phys.* **83,** 5013–5018 (1985).
10. Tannor, D. J., Kosloff, R. & Rice, S. A. Coherent pulse sequence induced control of selectivity of reactions: exact quantum mechanical calculations. *J. Chem. Phys.* **85,** 5805–5820 (1986).
11. Shapiro, M. & Brumer, P. Laser control of product quantum state populations in unimolecular reactions. *J. Chem. Phys.* **84,** 4103–4104 (1986).
12. Tannor, D. J. & Rice, S. A. Coherence pulse sequence control of product formation in chemical reactions. *Adv. Chem. Phys.* **70,** 441–523 (1988).
13. Brumer, P. & Shapiro, M. Laser control of molecular processes. *Annu. Rev. Phys. Chem.* **43,** 257–282 (1992).
14. Potter, E., Herek, J. L., Pedresen, S., Liu, Q. & Zewail, A. H. Femtosecond laser control of a chemical-reaction. *Nature* **355,** 66–68 (1992).
15. Fourkas, J. T., Wilson, W. L., Wäckerle, G., Frost, A. E. & Fayer, M .D. Picosecond time-scale phase-related optical pulses: measurement of sodium optical coherence decay by observation of incoherent fluorescence. *J. Opt. Soc. Am. B* **6,** 1905–1910 (1989).
16. Heberle, A. P., Baumberg, J. J. & Köhler, K. Ultrafast coherent control and destruction of excitations in quantum wells. *Phys. Rev. Lett.* **75,** 2598–2601 (1995).
17. Salour, M. M. & Cohen-Tannoudji, C. Observation of Ramsey's interference fringes in the profile of doppler-free two-photon resonances. *Phys. Rev. Lett.* **38,** 757–760 (1997).
18. Teets, R., Eckstein, J. & Hänsch, T. W. Coherent two-photon excitation by multiple light pulses. *Phys. Rev. Lett.* **38,** 760–764 (1977).
19. Blanchet, V., Nicole, C., Bouchene, M. & Girard, B. Temporal coherent control in two-photon transitions: from optical interferences to quantum interferences. *Phys. Rev. Lett.* **78,** 2716–2719 (1997).
20. Bellini, M., Bartoli, A. & Hänsch, T. W. Two-photon Fourier spectroscopy with femtosecond light pulses. *Opt. Lett.* **22,** 540–542 (1997).
21. Judson, R. S. & Rabitz, H. Teaching lasers to control molecules. *Phys. Rev. Lett.* **68,** 1500–1503 (1992).
22. Meshulach, D., Yelin, D. & Silberberg, Y. Adaptive ultrashort pulse compression and shaping. *Opt. Commun.* **138,** 345–348 (1997).
23. Yelin, D., Meshulach, D. & Silberberg, Y. Adaptive femtosecond pulse compression. *Opt. Lett.* **22,** 1793–1795 (1997).
24. Meshulach, D., Yelin, D. & Silberberg, Y. Adaptive real-time femtosecond pulse shaping. *J. Opt. Soc. Am. B* **15,** 1615–1619 (1998).
25. Bardeen, C. J. *et al.* Feedback quantum control of molecular electronic population transfer. *Chem. Phys. Lett.* **280,** 151–158 (1997).

Acknowledgements. We thank C. Cohen-Tannoudji, N. Davidson, T. W. Hänsch and D. Tannor for helpful discussions, D. Yelin for his help in developing pulse-shaping techniques and A. Arie for loan of the Cs cell.

Correspondence and requests for materials should be addressed to Y.S. (e-mail: feyaron@wis.weizmann.ac.il).

Observation of a square flux-line lattice in the unconventional superconductor Sr_2RuO_4

T. M. Riseman*, P. G. Kealey*, E. M. Forgan*, A. P. Mackenzie*, L. M. Galvin*, A. W. Tyler*, S. L. Lee†, C. Ager†, D. McK. Paul‡, C. M. Aegerter§, R. Cubitt‖, Z. Q. Mao¶, T. Akima¶ & Y. Maeno¶

** School of Physics and Astronomy, University of Birmingham, Birmingham B15 2TT, UK*
† School of Physics and Astronomy, University of St Andrews, St Andrews KY16 9SS, UK
‡ Department of Physics, University of Warwick, Coventry CV4 7AL, UK
§ Physik-Institut der Universität Zürich, CH-8057, Zurich, Switzerland
‖ Institut Laue-Langevin, F-38042, Grenoble, France
¶ Department of Physics, Kyoto University, Kyoto 606-8052, Japan

The phenomenon of superconductivity continues to be of considerable scientific and practical interest. Underlying this phenomenon is the formation of electron pairs, which in conventional superconductors do not rotate about their centre of mass ('*s*-wave' pairing; refs 1, 2). This contrasts with the situation in high-temperature superconductors, where the electrons in a pair are believed to have two units of relative angular momentum ('*d*-wave' pairing; ref. 3 and references therein). Here we report small-angle neutron-scattering measurements of magnetic flux lines in the perovskite superconductor Sr_2RuO_4 (ref. 4), which is a candidate for another unconventional paired electron state—'*p*-wave' pairing, which has one unit of angular momentum[5–7]. We find that the magnetic flux lines form a square lattice over a wide range of fields and temperatures, which is the result predicted by a recent theory[8,9] of *p*-wave superconductivity in Sr_2RuO_4. This theory also indicates that only a fraction of the electrons are strongly paired and that the orientation of the square flux lattice relative to the crystal lattice will determine which parts of the three-sheet Fermi surface of this material are responsible for superconductivity. Our results suggest that superconductivity resides mainly on the 'γ' sheet[9].

Strontium ruthenate (SRO) has nearly two-dimensional metallic properties, with a well-established Fermi surface[10–13] consisting of three sheets (α, β, γ). Non-*s*-wave superconductivity in this material is implied by the strong suppression of the superconducting transition temperature (T_c) below its maximum value of ~1.5 K by non-magnetic impurities, which thus act as pair-breakers[7]. Noting that the γ-sheet of the SRO Fermi surface is mainly derived from different Ru orbitals than are the α- and β-sheets, Agterberg *et al.*[8] have argued that pairing interactions will only weakly couple the different orbitals. They propose that *p*-wave superconductivity will be primarily present on either the γ-sheet, or the α- and β-sheets, with weak superconductivity on the other. This argument has been recently extended by Agterberg[9], who has shown that the flux-line lattice (FLL) structure for field perpendicular to the RuO_2 planes is very likely to be square, and that the orientation of the square flux lattice relative to the crystal lattice indicates which sheet(s) of the Fermi surface are primarily responsible for superconductivity. Thus, by observations of the flux lattice, we can gain important information about superconductivity in this material.

Neutron-diffraction patterns were obtained from the FLL in a sample of SRO (see Methods). A contour plot of a typical result is

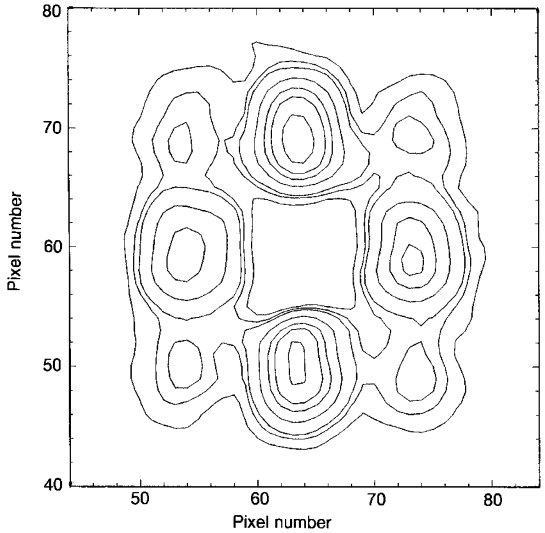

Figure 1 Contour plot of FLL diffraction pattern. With the geometry of our experiments, the diffracted neutrons form an image in the multidetector of the reciprocal lattice of the FLL: the central region of the detector has been masked. A field of 20 mT was applied parallel to **c** above T_c; data taken above T_c were subtracted from that obtained after cooling to 100 mK. The crystal **a** and **b** directions are horizontal and vertical in this figure. The sample shape causes the vertical spots to have different intensities from the horizontal ones, as discussed in Methods. The elongated shape of the spots reflects the shape of the exit aperture of the neutron guide.

shown in Fig. 1. The most notable feature of this pattern is that it is square, with the spots aligned with the **a**, **b** crystal axes, and that it certainly does not represent a triangular FLL. It should be noted that in addition to the $\{h,k\} = \{1,0\}$-type diffraction spots, higher-order {1,1} spots expected from a square FLL are observed in the expected positions; the intensity of the {1,1} spots is far too large for them to arise from multiple scattering. In Fig. 2, we show those regions of the B–T (magnetic induction-temperature) plane where we have established the existence of a square FLL in SRO; shortage of beamtime or weakness of the diffracted signal prevented a complete coverage of the relevant area of the plane, but we have no evidence of any departure from the square lattice structure. Of particular note is the result at 5 mT, which was obtained using an incident wavelength of 30 Å to detect the very long intervortex spacing of 0.64 μm. To our knowledge, this is the lowest-field FLL ever investigated by small-angle neutron scattering (SANS), and shows that there can be an overlap between this technique and decoration. A square FLL in SRO is also indicated by muon spin rotation (μSR) experiments in a purer sample than ours (G. M. Luke, personal communication), and in a less pure one[14]. The cumulative evidence of all these experiments is that in SRO a square FLL is widespread, and possibly intrinsic to its superconductivity.

It should be emphasised that with the field along the four-fold axis of the tetragonal structure of SRO, the original London or Ginzburg–Landau (GL) theories are necessarily isotropic[15], and hence predict a triangular rather than a square FLL. However, if non-local terms are added to the supercurrent response in the London theory[16], or higher-order gradient terms are added to the GL theory[17], then square FLLs can occur. Such theories tend to give a triangular flux lattice as T tends to T_c, where non-local effects become unimportant, and also at low magnetic inductions at all temperatures, because the response of any superconductor at long distances tends towards the London response. It appears that these approaches can explain the FLL transformations and square lattices seen in borocarbide superconductors in terms of Fermi surface anisotropy: see refs 17 and 18, and references therein. In general such effects are expected to be stronger in low-κ superconductors, which will have stronger interactions between the cores of adjacent flux lines. (The Ginzburg–Landau parameter is defined by $\kappa = \lambda/\xi$, where λ is the magnetic penetration depth and ξ is the coherence length.) It should also be noted that unconventional superconductivity is not necessarily implied by a square FLL: such a structure was also observed many years ago in a low-κ lead alloy[19]. However, another class of theories can also give rise to non-triangular lattices: these are extended GL theories, with more than one order parameter. For instance, d-wave superconductivity (with an s-wave component) in copper oxides is also expected to give rise to square FLLs[20]. Another example is the recent theory of p-wave superconductivity in SRO (ref. 9), which also leads to a square FLL. Using that theory (or indeed, a non-p-wave theory[16]), the relative orientation of the FLL and crystal lattice observed here implies that superconductivity in SRO resides principally in the γ-band electrons. This is not too surprising: we would expect this band to have the strongest pairing interaction, as it has the largest mass enhancement[13].

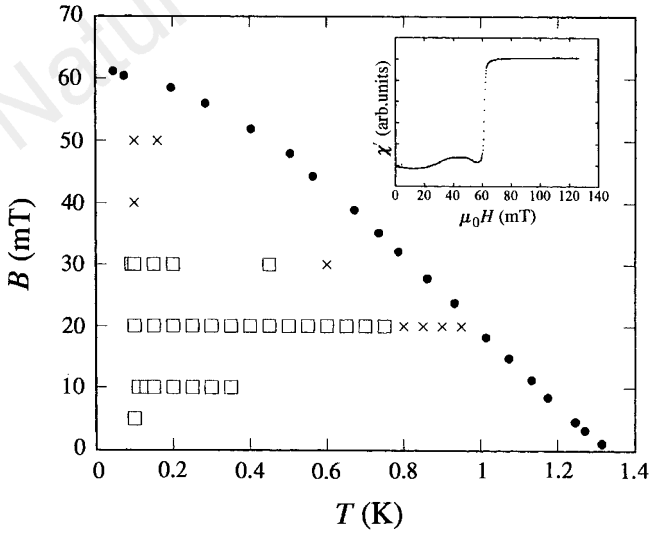

Figure 2 Observations in the B–T plane of a square FLL. By neutron scattering, a square FLL was observed at points marked with a square; at those marked with a cross, there was insufficient intensity to detect a FLL. The temperature dependence of B_{c2} for our sample with field parallel to **c** is also shown (filled circles). The transition was determined by measurement of the in-phase response of the a.c. susceptibility, χ'; a typical trace (at $T = 70$ mK) is shown as the inset.

To obtain further information about the properties of the superconductor, it is necessary to understand the intensity of the FLL signal, or equivalently, the magnitude of the Fourier components $|F_{hk}|$ of the magnetic field, described in Methods. In a high-κ superconductor, the London model is appropriate, and it gives $|F_{hk}|$ directly in terms of the temperature-dependent penetration depth, $\lambda(T)$, and hence the superfluid density, $n_S(T)$:

$$F_{hk}^{\text{London}} = \frac{B}{1 + q_{hk}^2\lambda^2(T)}, \quad \text{with } \frac{1}{\lambda^2(T)} \propto n_S(T) \tag{1}$$

Here $\mathbf{q}_{hk}$ are the reciprocal lattice wavevectors of the FLL. In a low-κ superconductor such as SRO, this will be modified by vortex core overlap. We choose to represent this by using the exact solution of the GL equations, calculated by the method of Brandt[21]. This gives $F_{hk}^{\text{GL}}/F_{hk}^{\text{London}}$ as a function $f(B/B_{c2})$, where f is weakly κ-dependent. In order to use this approach, we need the upper critical field B_{c2} (and the coherence length ξ from $B_{c2} = \Phi_0/2\pi\xi^2$, where Φ_0 is the flux quantum), which was determined as described in Methods and is plotted in Fig. 2.

Assuming the validity of the core overlap correction, we calculated a self-consistent set of λ and κ from the average integrated intensity of the horizontal spots. At 20 mT and 100 mK we obtain $\lambda = 194(16)$ nm and $\kappa = 2.6(2)$ ($f = 0.43$). Similar values have been obtained by μSR measurements (G. M. Luke, personal communication), and our value of κ is also supported by estimates of the critical field H_c from recent heat-capacity measurements on high-quality samples (S. NishiZaki and Y.M., unpublished data). The intensity of the weak {1,1} spots is difficult to separate from that of the {1,0} reflections, but appears to be somewhat larger than that given by the GL model with these parameters. We could not observe {2,0} reflections, and this is in accord with calculations of their expected intensity. It should be remembered that GL theory is only exact close to T_c and the calculations used a single-component order parameter, which may not be the case here. However, the mutual consistency of these results encourages us to believe that we have obtained reliable superconducting parameters for our sample.

We now compare our value of $B_{c2}(T = 0)$ with estimates from the Fermi surface properties, using the predictions of the BCS theory. With a cylindrical Fermi surface[22] for band i of radius k_F^i with carriers of effective mass $m = m_i^* m_e$, where m_e is the electron mass:

$$B_{c2}(0) = \frac{2\pi}{\gamma}\Phi_0\left(\frac{k_B T_c m_e}{\hbar^2}\right)^2\left(\frac{m_i^*}{k_F^i}\right)^2 \tag{2}$$

Here $\ln(\gamma)$ is Euler's constant (0.577); we note that this equation is slightly different from the standard BCS result, which is for a spherical Fermi surface. We have included a band index i as the Fermi surface in SRO consists of three bands. As suggested elsewhere[23], the value of $B_{c2}(0)$ in a multi-band superconductor will be controlled by the band giving the highest value. The calculated values are shown in Table 1, and it is clear that the γ-band is in surprisingly good agreement with our observations. These values strongly suggest that at least in high fields, the super-

Table 1 Fermi surface properties and superconducting parameters of Sr_2RuO_4

	α (holes)	β (electrons)	γ (electrons)
k_F^i (Å^{-1}) (ref. 10)	0.302(2)*	0.621(3)	0.750(4)
N_i (ref. 10)	0.216(2)	0.914(9)	1.334(13)
m_i^*	3.4(2)	7.5(4)	14.6(7)
m_i^*/k_F^i	11.3(6)	12.1(6)	19.5(10)
N_i/m_i^*	0.064(3)	0.122(6)	0.091(5)
$B_{c2}(0)$ (mT) Eq. (2)	19(2)	22(2)	58(6)
$\lambda_L(0)$ (nm) Eq. (3)	$\alpha+\beta+\gamma$: 98(2)†		
$\lambda_L(0)$ (nm)	$\alpha+\beta$: 120(3)		γ: 171(4)
λ_L (experiment)	194(16) nm: from SANS at 100 mK		
$B_{c2}(0)$ (experiment)	63 mT: from a.c. measurements		

Values of m_i^* are revised values from ref. 13.
* Error in last figure in parentheses.
† Value using all three bands and $V_M = 5.71 \times 10^{-5}$ m^3 (ref. 32).

conductivity of SRO is mainly due to the γ-band, because one would expect the other bands to be depaired at these fields. (However, it should be noted that more exotic pairing could alter the numerical factors in equation (2).)

We can also calculate the low-temperature value of the penetration depth $\lambda(0)$ from the Fermi surface properties, and compare this with λ from the SANS results. The free-electron expression is: $1/\lambda^2(0) = ne^2\mu_0/m_e$, where n is the electron density. If there are several bands, this generalizes (for either spherical or cylindrical Fermi surfaces) to:

$$\frac{1}{\lambda^2(0)} = \frac{e^2\mu_0}{m_e}\sum_i \frac{n_i}{m_i^*} = \frac{N_A e^2 \mu_0}{V_M m_e}\sum_i \frac{N_i}{m_i^*} \qquad (3)$$

where N_i is the number of electrons per formula unit in band i and V_M/N_A is the volume of one formula unit. Table 1 shows the result of applying equation (3) to all three bands: the value of λ comes out much smaller than our low-temperature experimental value. Now λ represents the strength of Meissner screening at long distances, and it depends only on the response of the electronic charges to the magnetic vector potential **A**, and not on the nature of the pairing. It can be shown[24] that all parts of the Fermi surface that have a gap contribute to the low-temperature value of λ. It seems clear that reasonable agreement with our other results can only be obtained by assuming that under the conditions of our experiment only the γ-surface contributes significantly to λ.

All our results are consistent with ideas of orbital-dependent p-wave superconductivity[8,9]. Within that framework, a non-time-reversal-invariant superconducting state is expected[9], and has recently been observed[25]. We briefly discuss alternative schemes. One is a "non-unitary" pairing state[26,27], which also breaks time-reversal symmetry and can have nodes in the gap. However, such a state only occurs (as seen in the A1 phase of ^{3}He) if some extra stabilizing factor such as strong coupling is present[26]. Estimates of the coupling strength[28] make this state unlikely. We should also consider d-wave pairing: however, to break time-reversal symmetry all the way to T_c, one needs two degenerate states, and the only candidate (Γ_5^+ in the nomenclature of table IV in ref. 29) has nodes on the Fermi surface, where the z-component of the wavevector k_z is zero. Such a k_z-dependence of the gap is not expected in a two-dimensional material such as SRO. We conclude that the symmetry and orientation of the FLL and the values of the superconducting parameters all indicate that superconductivity in strontium ruthenate occurs primarily on the γ-sheet of the Fermi surface, and that the p-wave model[8,9] gives the most consistent explanation of our results as a whole. □

Methods

Sample preparation and properties. The sample of Sr_2RuO_4 was grown by the floating-zone technique with excess RuO_2 as a flux[30]. It formed a rod of approximately elliptical cross-section (2.5 × 3.5 mm), with the **c**-direction of the tetragonal structure (perpendicular to the RuO_2 planes) along the short axis of the ellipse, and one of the **a/b** directions ~30° from the axis of the rod. T_c was 1.28 K (mid-point) with width (10–90%) of ~60 mK, measured by low-frequency a.c. susceptibility. The highest T_c so far obtained in this material is 1.48 K, so our sample was subject to a small (~15%) depairing by the residual electron scattering.

SANS techniques. A length of 8 mm was diamond-cut from the growth rod; this was held mechanically, and by a small quantity of glue, to a copper plate, mounted on the mixing chamber of a dilution refrigerator. This was placed between the poles of an electromagnet with holes parallel to the field for transmission of neutrons. The magnetic field was parallel to the **c**-axis of the crystal within 0.5°, and the FLL was observed using long-wavelength neutrons, incident nearly parallel to the applied field, on instrument D22 at the Institut Laue Langevin. Typical wavelengths employed were 14 Å, with a spread (full-width at half-maximum) of 12%. Transmitted neutrons were registered at a 128 × 128 pixel multidetector (pixel size 7.5 × 7.5 mm) 17.71 m beyond the sample. The main beam was intercepted by a Cd beamstop and the weak diffracted beams due to the FLL were extracted from the background scattering from sample and cryostat by subtracting data taken above T_c.

Measurement of integrated intensity. Integrated intensities of FLL diffraction spots lying in the horizontal plane could be measured by rotating the electromagnet and the sample together about a vertical axis, rocking these spots through the Bragg condition. The integrated intensity I_{hk} of a (h, k) reflection with wavevector q_{hk} may be related to a Fourier component F_{hk} of the magnetic field variation inside the FLL, via the relationship: $I_{hk} = 2\pi\phi(\mu/4)^2(V\lambda_n^2/\Phi_0^2 q_{hk})|F_{hk}|^2$, where ϕ is the incident flux of neutrons of wavelength λ_n, V is the sample volume, Φ_0 is the flux quantum and μ is the neutron magnetic moment in nuclear magnetons. In initial measurements, we formed the FLL by cooling the sample in constant applied field. This gave a rather broad rocking-curve width of several degrees, which reduced the peak intensity and made the integration for I_{hk} inaccurate. We suspect that the width was due to random pinning and bending of the flux lines into a non-optimum configuration (the large anisotropy of SRO will make the flux lines particularly easy to bend). In $NbSe_2$, another anisotropic superconductor, the quality of the FLL under such circumstances was improved by passing a current[31]. We therefore induced currents in our sample by oscillating the applied field by ±1 mT at ~0.5 Hz during cooling. This increased the peak diffracted intensity by a factor ~2 and the rocking-curve width was reduced to ~1.5° half-width at half-maximum (the integrated intensity should be unchanged). The diffraction pattern shown in Fig. 1 was observed after cooling in this manner. The rocking-curve width was still large compared with the Bragg θ for all the diffracted spots, so the complete pattern is seen with the incident neutron beam parallel to the field. It will be noted that the vertical spots are ~1.6 times more intense than the horizontal spots: we believe that this is because with a (nearly vertical) rod-shaped sample, most residual flux-line bending will be in the horizontal direction.

Measurement of B_{c2}. This was determined from the a.c. susceptibility (0.2 mT at 97 Hz applied parallel to **c**) of a small piece cut from the growth rod immediately adjacent to the SANS sample, as a function of temperature and magnetic field B applied parallel to the crystal **c**-axis. A typical in-phase response as a function of magnetic field (swept up or down) at constant temperature is shown in Fig. 2 inset. At low levels of excitation the flux lines are pinned, so a strong diamagnetic response is seen as soon as the sample enters the mixed state from the normal state. B_{c2} is taken as the mid-point of the a.c. transition.

Received 25 June; accepted 18 August 1998.

1. Bardeen, J., Cooper, L. N. & Schrieffer, J. R. Theory of superconductivity. *Phys. Rev.* **108,** 1175–1204 (1957).
2. Anderson, P. W. & Morel, P. Generalised Bardeen-Cooper-Schrieffer states and the proposed low temperature phase of liquid He^3. *Phys. Rev.* **123,** 1911–1934 (1961).
3. Tsuei, C. C. & Kirtley, J. R. Phase-sensitive tests of pairing symmetry in cuprate superconductors. *Physica C* **282,** 4–11 (1997).
4. Maeno, Y. *et al.* Superconductivity in a layered perovskite without copper. *Nature* **372,** 532–534 (1994).
5. Rice, T. M. & Sigrist, M. Sr_2RuO_4: an electronic analogue of ^{3}He? *J. Phys: Condens. Matter* **7,** L643–648 (1995).
6. Maeno, Y. Electronic states of the superconductor Sr_2RuO_4. *Physica C* **282-7,** 206–209 (1997).
7. Mackenzie, A. P. *et al.* Extremely strong dependence of superconductivity on disorder in Sr_2RuO_4. *Phys. Rev. Lett.* **80,** 161–164 & (erratum) 3890 (1998).

8. Agterberg, D. F., Rice, T. M. & Sigrist, M. Orbital dependent superconductivity in Sr_2RuO_4. *Phys. Rev. Lett.* **78,** 3374–3377 (1997).
9. Agterberg, D. F. Vortex lattice structures of Sr_2RuO_4. *Phys. Rev. Lett.* **80,** 5184–5187 (1998).
10. Mackenzie, A. P. *et al.* Quantum oscillations in the layered perovskite superconductor Sr_2RuO_4. *Phys. Rev. Lett.* **76,** 3786–3789 (1996).
11. Maeno, Y. & Yoshida, K. Fermi liquid properties and superconductivity of Sr_2RuO_4. *Czech. J. Phys.* **46,** Suppl. S6, 3097–3104 (1996).
12. Maeno, Y. *et al.* Two-dimensional Fermi liquid behavior of the superconductor Sr_2RuO_4. *J. Phys. Soc. Jpn* **66,** 1405–1408 (1997).
13. Mackenzie, A. P. *et al.* Fermi surface topography of Sr_2RuO_4. *J. Phys. Soc. Jpn* **67,** 385–388 (1998).
14. Aegerter, C. M. *et al.* Evidence for a square vortex lattice in Sr_2RuO_4 by muon-spin rotation measurements. *J. Phys: Condens. Matter* **10,** 7445–7451 (1998).
15. Hohenberg, P. C. & Werthamer, N. R. Anisotropy and temperature dependence of the upper critical field of type-II superconductors. *Phys. Rev.* **153,** 493–497 (1967).
16. Kogan, V. G. *et al.* Vortex lattice transitions in borocarbides. *Phys. Rev. B* **55,** 8693–8696 (1997).
17. De Wilde, Y. *et al.* The superconducting energy gap and vortex lattice structure in $LuNi_2B_2C$. *Physica C* **282-7,** 355–358 (1997).
18. Paul, D. McK. *et al.* Nonlocal effects and vortex lattice transitions in YNi_2B_2C. *Phys. Rev. Lett.* **80,** 1517–1520 (1998).
19. Obst, B. Rectangular flux line lattice in type II superconductors. *Phys. Lett A* **28,** 662–663 (1969).
20. Berlinsky, A. J., Fetter, A. L., Franz, M., Kallin, C. & Soininen, P. I. Ginzburg-Landau theory of vortices in d-wave superconductors. *Phys. Rev. Lett.* **75,** 2200–2203 (1995).
21. Brandt, E. H. Precision Ginzburg-Landau solution of ideal vortex lattices for any induction and symmetry. *Phys. Rev. Lett.* **78,** 2208–2211 (1997).
22. Schofield, A. J. Upper critical-field in the gauge-model. *Phys. Rev. B* **51,** 11733–11738 (1995).
23. Mackenzie, A. P. *et al.* Calculation of thermodynamic and transport-properties of Sr_2RuO_4 at low-temperatures using known Fermi-surface parameters. *Physica C* **263,** 510–515 (1996).
24. Rickayzen, G. in *Superconductivity* (ed. Parks, R. D.) 91 (Dekker, New York, 1969).
25. Luke, G. M. *et al.* Time-reversal symmetry breaking superconductivity in Sr_2RuO_4. *Nature* **394,** 558–561 (1998).
26. Sigrist, M. & Zhitomirsky, M. E. Pairing symmetry of the superconductor Sr_2RuO_4. *J. Phys. Soc. Jpn* **65,** 3452–3455 (1996).
27. Machida, K., Ozaki, M. & Ohmi, T. Odd-parity pairing superconductivity under tetragonal symmetry—possible application to Sr_2RuO_4. *J. Phys. Soc. Jpn* **65,** 3720–3723 (1996).
28. Mazin, I. I. & Singh, D. Ferromagnetic spin fluctuation induced superconductivity in Sr_2RuO_4. *Phys. Rev. Lett.* **79,** 733–736 (1997).
29. Sigrist, M. & Ueda, K. Phenomenological theory of unconventional superconductivity. *Rev. Mod. Phys.* **63,** 239–311 (1991).
30. Maeno, Y., NishiZaki, S., Yoshida, K., Ikeda, S. & Fujita, T. Normal-state and superconducting properties of Sr_2RuO_4. *J. Low. Temp. Phys.* **105,** 1577–1588 (1996).
31. Yaron, U. *et al.* Structural evidence for a 2-step process in the depinning of the superconducting flux-line-lattice. *Nature* **376,** 753–755 (1996).
32. Chmaissem, O., Jorgensen, J. D., Shaked, H., Ikeda, S. & Maeno, Y. Thermal expansion and compressibility of Sr_2RuO_4. *Phys. Rev. B* **57,** 5067–5070 (1998).

Acknowledgements. We thank J.-L. Ragazzoni of the ILL for setting up the dilution refrigerator, D. F. Agterberg for useful discussions, E. H. Brandt for giving us a copy of his program and G. M. Luke for communicating results before publication. One of us (A.P.M.) acknowledges the support of the Royal Society. This work was supported by the UK EPSRC, and CREST of Japan Science and Technology Corporation. The neutron scattering was carried out at the Institut Laue-Langevin, Grenoble.

Correspondence and requests for materials should be addressed to T.M.R. (e-mail: tmr@th.ph.bham.ac.uk).

Surface-promoted replication and exponential amplification of DNA analogues

A. Luther, R. Brandsch & G. von Kiedrowski

Lehrstuhl für Bioorganische Chemie, Ruhr-Universität Bochum, Universitätstrasse 150, NC 2/173, D-44780 Bochum, Germany

Self-replicating chemical systems have been designed and studied to identify the minimal requirements for molecular replication[1], to translate the principle into synthetic supramolecular systems[2] and to derive a better understanding of the scope and limitations of self-organization processes[3] that are believed to be relevant to the origin of life on Earth[4]. Current implementations make use of oligonucleotide analogues[5–12], peptides[13–17], and other molecules[18–24] as templates and are based either on autocatalytic, cross-catalytic, or collectively catalytic pathways for template formation. A common problem of these systems is product inhibition, leading to parabolic instead of exponential amplification[25]. The latter is the dynamic prerequisite for selection in the darwinian sense[26,27]. We here describe an iterative, stepwise procedure for chemical replication which permits an exponential increase in the concentration of oligonucleotide analogues. The procedure employs the surface of a solid support and is called SPREAD (surface-promoted replication and exponential amplification of DNA analogues). Copies are synthesized from precursor fragments by chemical ligation on immobilized templates, and then liberated and immobilized to become new templates. The process is repeated iteratively. The role of the support is to separate complementary templates which would form stable duplexes in solution. SPREAD combines the advantages of solid-phase chemistry with chemical replication, and can be further developed for the non-enzymatic and enzymatic amplification of RNA, peptides and other templates as well as for studies of *in vitro* evolution and competition in artificial chemical systems. Similar processes may also have played a role in the origin of life on Earth, because the earliest replication systems may have proliferated by spreading on mineral surfaces[28–33].

Stepwise 'feeding' procedures were previously employed in two different chemical systems that were reported as models of potentially prebiotic processes[10,34,35]. Li and Nicolaou achieved chemical replication of duplex DNA composed of palindromic (symmetrical) homopyrimidine and homopurine strands[10]. The homopyrimidine strand was synthesized from its precursor fragments via triple helix ligation, and then served as a template for the chemical ligation of the precursors of the homopurine strand. Thus, stepwise feeding with homopyrimidine and homopurine fragments prevented fragment complexation and therefore allowed switching between the respective triplex and duplex ligation intermediates. Ferris *et al.* have demonstrated the synthesis of long oligonucleotide- and peptide-like materials on the surface of mineral supports[34,35]. In these systems, stepwise feeding enabled the replenishment of activated precursors, and thus overcame the length-limiting effect of precursor hydrolysis. The conjunction of the above approaches, stepwise chemical replication and solid-phase chemistry, forms the basis of our procedure (Fig. 1).

For a demonstration of SPREAD (Fig. 2), two complementary 14-meric templates, **X** and **Y**, as well as four template fragments, $\mathbf{A}^x$, $\mathbf{B}^x$, $\mathbf{A}^y$ and $\mathbf{B}^y$, were synthesized using standard phosphoramidite chemistry. A thiol-modified support was obtained from

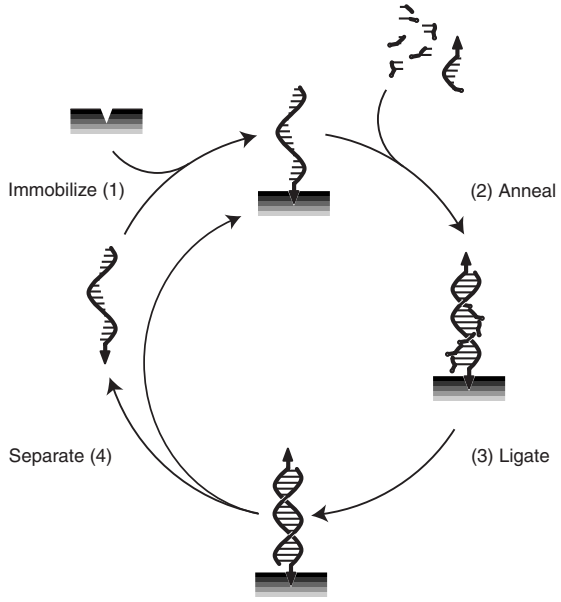

Figure 1 General scheme of the SPREAD procedure. (1) A template is immobilized by an irreversible reaction with the surface of a solid support. (2) The template binds complementary fragments from solution. (3) The fragments are linked together by chemical ligation. (4) The copy is released, and re-immobilized at another part of the solid support to become a template for the next cycle of steps. Irreversible immobilization of template molecules is thus a means to overcome product inhibition.